Observation of two distinct negative trions in tungsten disulfide monolayers

Abdelaziz Boulesbaa,* Bing Huang, Kai Wang, Ming-Wei Lin, Masoud Mahjouri-Samani, Christopher Rouleau, Kai Xiao, Mina Yoon, Bobby Sumpter, Alexander Puretzky, and David Geohegan

Center for Nanophase Materials Sciences, Oak Ridge National Laboratory, 1 Bethel Valley Road, Oak Ridge, Tennessee, 37831, USA

(Received 29 April 2015; revised manuscript received 28 August 2015; published 25 September 2015)

Ultrafast pump-probe spectroscopy of two-dimensional tungsten disulfide monolayers (2D WS_2) grown on sapphire substrates revealed two transient absorption spectral peaks that are attributed to distinct negative trions at ∼2.02 eV (T_1) and ∼1.98 eV (T_2). The dynamics measurements indicate that trion formation by the probe is enabled by photodoped 2D WS_2 crystals with electrons remaining after trapping of holes from excitons or free electron-hole pairs at defect sites in the crystal or on the substrate. Dynamics of the characteristic absorption bands of excitons X_A and X_B at ∼2.03 and ∼2.40 eV, respectively, were separately monitored and compared to the photoinduced absorption features. Selective excitation of the lowest exciton level X_A using $\lambda_{pump} < 2.4$ eV forms only trion T_1, implying that the electron remaining from dissociation of exciton X_A is involved in the creation of this trion with a binding energy ∼10 meV with respect to X_A. The absorption peak corresponding to trion T_2 appears when $\lambda_{pump} < 2.4$ eV, which is just sufficient to excite exciton X_B. The dynamics of trion T_2 formation are found to correlate with the disappearance of the bleach of the X_B exciton, indicating the involvement of holes participating in the bleach dynamics of exciton X_B. Static electrical-doping photoabsorption measurements confirm the presence of an induced absorption peak similar to that of T_2. Since the proposed trion formation process here involves exciton dissociation through hole trapping by defects in the 2D crystal or substrate, this discovery highlights the strong role of defects in defining optical and electrical properties of 2D metal chalcogenides, which is relevant to a broad spectrum of basic science and technological applications.

DOI: 10.1103/PhysRevB.92.115443 PACS number(s): 71.35.−y, 73.21.−b, 78.47.J−

I. INTRODUCTION

A hydrogen ion composed of one proton bound to two electrons can be considered as a prototype of a negative trion [1]. Similarly, a positive trion is prototyped by a helium cation where one electron is bound to two protons [1]. In semiconductors, and particularly two-dimensional transition metal dichalcogenide monolayers (2D TMDs), trions arise from charging bound electron-hole pairs (excitons) [2–9]. After their predicted existence in bulk semiconductors in the late 1950s [4], the journey toward observing them took almost two decades [9]. With the development of confined nanostructures in the 1990s, both positive and negative trions with binding energies on the order of a few meV were observed in semiconductor quantum wells [2,3]. Since the discovery of graphene in 2004 [10], two-dimensional layered materials in general, and 2D TMDs in particular, became a popular platform for many-body physics exploration. In fact, trions with binding energies as high as 20−40 meV were recently observed in these materials [5–8]. In 2D TMDs, optical and electrical properties essentially arise from two intrinsic properties: the breaking of inversion symmetry and quantum confinement in one direction. For instance, the valley and spin Hall effects result due to the breaking of inversion symmetry in 2D TMDs through the application of in-plane electric fields [11,12]. As a result, the selection rules of optical transitions become valley dependent, which is at the heart of spintronic applications [13]. In addition, quantum confinement within a monolayer thickness enhances the Coulomb interaction between holes in the valence band (VB) and electrons in the conduction band (CB). Consequently, the optical and electrical properties become dominated by excitonic effects, which makes these materials an excellent platform to explore many-body physics, contrary to bulk 3D materials where optical and electrical properties are dominated by charged free carriers [5].

Although there is a current consensus, in both the computational and experimental research communities, that in 2D TMDs there are two band-edge exciton states X_A and X_B, only one trion state T_1 has yet been observed bound by ∼10−30 meV with respect to the exciton state X_A [5,14]. Here, through ultrafast pump-probe spectroscopy dynamics, we report the observation of two distinct trion states: a trion state T_1 associated with the photoformation of exciton X_A, and a second trion state T_2 observed only when the pump photon energy is greater than 2.4 eV, just sufficient to produce exciton X_B. The formations of trion states T_1 and T_2 are revealed in pump-probe spectroscopy as induced absorptions enabled by n-type photodoping of 2D WS_2 crystals with electrons remaining after exciton creation, and dissociation through hole-trapping at substrate or defect sites. We correlate the dynamic formation of these two trion states arising from spin-orbit splitting in the crystal. Our ultrafast pump-probe approach allows the detection of very small transient absorptions/depletions induced by the pump and the separation of different processes based on their decay dynamics, which makes possible the observation of trions with very low binding energy, even at room temperature. The results indicate that although X_B is produced through the excitonic transition corresponding to the bottom spin-orbit-split (SOS) level in the valence band (V_2) and the bottom SOS level in the conduction band (C_1), the spectral position of the new T_2 band does not correlate with that of the X_B transition ($V_2 - C_1$) but correlates instead with a trion state with a binding energy of ∼17 meV with respect to a "dark exciton" corresponding to a transition (V_1-C_1) that is

*Author to whom correspondence should be addressed: boulesbaaa@ornl.gov

forbidden by spin selection rules. We report that since T_1 and T_2 share the same V_1 energy level in the VB, their formation is subject to competition dictated by the Pauli principle.

II. METHODS

Preparation of 2D WS_2 monolayers. Monolayers of WS_2 were synthesized by low-pressure chemical vapor deposition (CVD) on sapphire substrates (crystal cut at plane [0001]) according to the reported procedure in the literature [15]. Briefly, tungsten trioxide (WO_3) powder was placed in an alumina crucible located at the heating zone center of a 2-in. horizontal tube furnace. After consecutive cleaning by acetone/isopropanol/deionized water, the substrate was also loaded downstream next to WO_3 powder in the same crucible. The sulfur powder was placed in a separate crucible at the upstream side where the temperature was around 160 °C during the growth. The furnace was heated first to 600 °C, then 900 °C, with ramping rates of 25 °C/min and 10 °C/min, respectively. After the temperature was kept at 900°C for 25 min, the furnace was turned off and allowed to cool to room temperature. A constant Ar/H_2 gas [Ar = 60 SCCM (SCCM denotes cubic centimeters per minute at STP), H_2 = 10 SCCM) was introduced into the tube furnace reactor and the pressure was maintained at 500 mTorr during the whole growth procedure. Similarly, monolayers of WS_2 were also grown on 300-nm-thick SiO_2 on Si substrates with the same setup but at ambient pressure of argon. The temperature of the furnace center was ramped to 800 °C at 20 °C/min with 50 SCCM Ar, maintained at 800 °C for 20 min, and then cooled down naturally with 200 SCCM gas flow. To ensure a continuous sulfur vapor supply, a heating tape was used to heat the crucible containing sulfur upstream of the furnace entrance to 120°C during the growth.

Simulations. First-principles density functional theory (DFT) calculations were performed with the Vienna *ab initio* package (VASP) [16]. The generalized gradient approximation with the Perdew-Burke-Ernzerhof (PBE) functional for the exchange correlation potential and the projector augmented wave (PAW) method are adopted. Fourteen and six valence electrons are included for W and S potentials, respectively. The GW versions of the potentials, which are designed to provide improved scattering properties at high energies, are employed for all atoms. The kinetic energy cutoff was 500 eV. A vacuum slab of 20 Å was selected to simulate single-layer WS_2, which was sufficient to ensure minimal interlayer coupling. For Brillouin zone integration, an $18 \times 18 \times 1$ Γ-centered K-point mesh was used. Employing self-consistent charge density from the DFT run, we perform a subsequent non-self-consistent spin-orbit coupling (SOC) calculation in the spirit of perturbation theory. In GW calculations, single-shot $G0W0$ calculation was performed [17] including 192 conduction bands and the energy cutoff for the response function of 300 eV . The convergence of our calculations is checked by increasing the empty bands to 384 and the K-point density to $24 \times 24 \times 1$. The BSE optical spectrum and optical transition calculations were carried out on top of Self-Consistent GW. The eight highest valence bands and the eight lowest conduction bands were included as basis for the excitonic state, which was sufficient to converge the energies of X_A and X_B excitonic peaks. The Bethe-Salpeter Equation (BSE) was solved using the Tamm-Dancoff approximation.

Time-resolved spectroscopy measurements. A home-built femtosecond pump-probe spectrometer (PPS) was used to measure ultrafast exciton dynamics in WS_2 monolayers. The PPS is based on a titanium sapphire (Ti:Sa) oscillator (Micra, Coherent) with its output seeding a Ti:Sa Coherent Legend (USP-HE) amplifier operating at 1kHz repetition rate. The Legend amplifier provides pulses centered at 800 nm, with 40 fs duration and 2.2 μJ energy per pulse. The output of the Legend amplifier was divided onto two portions: 90% was used to generate tunable excitation pulses in an optical parametric amplifier (TOPAS, Coherent), and the second portion (10%) was used to generate the white light continuum (WLC) probe in a 2-mm-thick sapphire window. The WLC which covers the spectral range from 450 to 900 nm was collimated and focused using parabolic mirrors to minimize temporal chirp. The transmitted WLC after the sample was sent for detection through a 100-μm-core optical fiber coupled with a spectrometer-linear CCD array (USB2000ES, Ocean Optics). The pump beam was sent through a controllable optical delay line and was chopped at 500 Hz frequency to allow absorption changes in the transmitted probe to be measured between every two successive laser shots. At every time delay, 200 absorbance changes were averaged unless mentioned otherwise. At the sample, the probe and pump spot sizes were $\sim$50 and $\sim$100 μm, respectively. A scheme representative for the experimental setup is depicted in Fig. S1 in the Supplemental Material [18]. In order to avoid photodamaging of 2D WS_2 monolayers, the pump fluence at the sample was kept below 2 $\mu J/cm^2$ using one neutral density filter. Assuming that every absorbed photon generates one exciton, the density of generated excitons is estimated to be on the order of $\sim 10^{11}/cm^2$. An additional tunable neutral density filter was used to slightly adjust the intensity of excitation to produce the same maximum bleach signal size at the lowest exciton X_A upon excitation at different energies. For all excitation energies used in this work, the sample was not photodamaged based on the reproducibility of both signal size and dynamics from one scan to another, and from day to day. Additionally, it is important to note that all measurements were carried out at ambient temperature, and both pump and probe polarizations were kept linear and parallel to the 2D monolayer surface.

For single-crystal measurements, the pump and probe beams are sent to the sample collinearly and focused down to sub-10-μm spot sizes with a 15× reflective objective. The reflected probe is detected by a spectrometer (Shamrock 303i, Andor) equipped with an electron multiplier (EM) CCD (Newton, Andor).

Electro-optical spectroscopy measurements. In this experiment, a white light beam was focused with a microscope objective on a single 2D WS_2 flake on a silicon substrate separated by a 300 nm thin layer of silica (SiO_2). A layer of titanium (5 nm) and gold (30 nm) was deposited on the 2D WS_2 in one side, and on the back side of the silicon substrate. The two electrodes were connected to a Keithley 2400 source meter. The reflected white light was focused on an entrance slit of a spectrograph (Acton Research) equipped with a CCD detector (Princeton Instruments) as shown in the left panel of Fig. 3. The absorbance change between absence

of applied voltage (I_0) and nonzero applied voltage (I_V) was calculated by monitoring the intensity of the reflected light (I) as $\Delta A = -\log_{10}(I_V/I_0)$.

III. RESULTS AND DISCUSSION

The absorption spectrum of monolayer WS_2 crystals grown by CVD on a sapphire substrate (Fig. S2(a) in the Supplemental Material [18]) shows three distinct peaks around 2.03, 2.43, and 2.91 eV superimposed on a broad absorption band (Fig. S3). Similar to bulk WS_2 and other transition metal dichalcogenide crystals [19]. These peaks were attributed to excitons X_A, X_B, and X_C, respectively [5,6,20]. The band-edge excitons X_A and X_B arise from transitions between spin-orbit-split levels in the valence band maximum and conduction band minimum as illustrated in Fig. 1(a). For instance, at the K valley, $X_A(X_B)$ is formed between a hole at $V_1(V_2)$ with spin up (down) and an electron at $C_2(C_1)$ with spin down (up) [8,21,22]. Extensive studies of

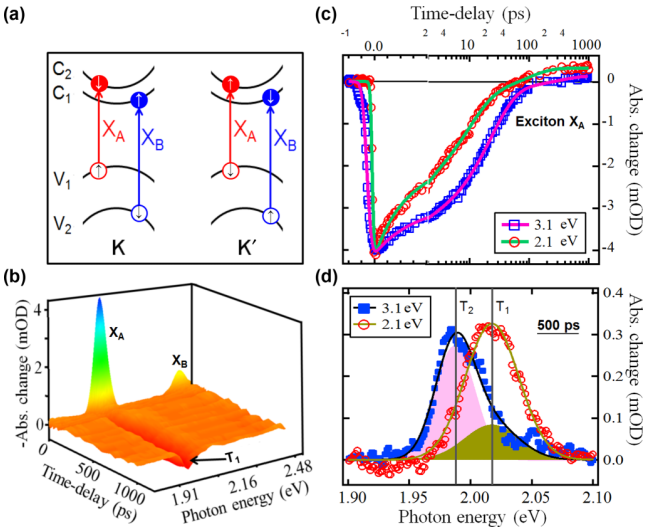

FIG. 1. (Color online) **Band-edge optical transitions in 2D-WS_2.** (**a**), Schematic representation of the lowest excitonic transitions X_A and X_B at the K-point and $K' = -K$ point. Spin states are indicated by small "up" and "down" arrows. (**b**), Transient absorption 3-D plot upon excitation at 2.1 eV. Because 2.1 eV excitation is insufficient for X_B(2.4 eV) generation, the observed depletion of the X_B transition is due to a state-filling effect rather than generation of X_B (see Fig. S5 and corresponding supplementary text). (**c**), X_A bleach dynamics upon excitation at different energies (symbols) fitted to a bi-exponential function (solid lines). One fast component describes the hot carriers relaxation, and the second component describes electron-hole recombination. A third component to describe the positive portion of the signal was added (+0.6 and +0.2 mOD in case of 2.1 and 3.1 eV excitations, respectively). The fitting parameters are listed in Table S1. (**d**), TAS recorded 500 ps after excitation as indicated. In the case of excitation at 2.1 eV, the spectrum (open circles) was fit to one Gaussian describing T_1 (olive solid line). During the fit of the measured spectrum (filled squares) in the case of excitation at 3.1 eV with the sum of two Gaussians (solid dark line), the center and the width of T_1 were fixed, but the center and the width of T_2 were returned by the converged fit (shaded areas). The fitting parameters are listed in Table S6.

the binding energies of these excitons in a monolayer WS_2 have been conducted using linear reflectance spectroscopy at low temperatures, resulting in 0.32 eV X_A binding energy [5], and two-photon photoluminescence excitation spectroscopy which gave 0.7 eV binding energy for X_A excitons [6,20]. The existing difference in the measured binding energies by different groups has been explained recently with the conclusion that these two different numbers correspond to the onsets of the band gaps of two different excitons X_A (∼2.4 eV) and X_B(∼2.8 eV) [23]. Theoretical attempts to explain the broad absorption continuum in similar 2D MoS_2 crystals showed a possible large number of other strongly bound excitonic states between X_B and X_C broadened due to electron-phonon interaction that might explain the origin of the broadband absorption [24]. We also calculated the energy bands and lowest excitonic transitions in 2D WS_2 monolayers using GW plus the Bethe-Salpeter equation (GW-BSE) [see Fig. S2(b) in [18]]. Depicted in Fig. 1(a) are the four energy levels resulting from spin-orbit splitting at the conduction band minimum (CBM) and valence band maximum (VBM) at the K and $K' = -K$ points. These levels are associated with two optically active excitonic transitions X_A(∼2.03 eV) and X_B (∼2.40 eV).

To understand the dynamics of these band-edge excitons, ensembles of 3−5μm 2D WS_2 monolayer crystals were probed by femtosecond pump-probe spectroscopy. It should be noted that we used a multicrystalline monolayer WS_2 sample with the 50 μm probe beam covering multiple individual crystals, including their edges and grain boundaries. Recently it has been reported that excitons from the crystal edges are redshifted (∼50 meV) compared to excitons from flake centers [25]. Consequently, this sample provides ensemble information on the position of quasiparticle absorption bands due to contributions from the flake centers and edges that lead to spectral shifts and broadening. Comparison with transient absorption measurements from the center of large (∼40 μm)WS_2 single crystals grown on SiO_2/Si substrates is given in Fig. S4 in [18].

2D WS_2 monolayers were excited at 2.1 and 3.1 eV by the pump beam, and the temporal evolutions of X_A and X_B bleach formations and recoveries were tracked by the probe pulse. Transient absorption spectra (TAS) resulting from excitation at 2.1 eV demonstrated the subpicosecond formation of excitons X_A and X_B [Fig. 1(b)]. The time required for the bleach of X_A to reach its maximum amplitude was about 500 fs longer in the case of excitation at 3.1 eV [Fig. 1(c)]. This delay is related to the intraband relaxation from higher excited states populated with the 3.1 eV pump laser to the lowest excitonic state X_A. This has been observed previously for MoS_2 monolayers [26]. Figure 1(c) shows that the bleach recovery of X_A was faster (∼9 ps) in the case of the 2.1 eV pump compared to that for 3.1 eV(∼22 ps) (see Table S1 in [18]). This suggests the possibility of a quenching pathway of X_A that is more efficient in the case of near-resonance excitation of X_A.

To investigate the reason for the X_A bleach lifetime dependence on the excitation photon energy, TAS collected at 500 ps time delays upon excitation at 2.1 and 3.1 eV were closely examined [Fig. 1(d)]. In the case of excitation at 2.1 eV, the spectrum shows an induced absorption [T_1 in Figs. 1(b) and 1(d)] at the "red" side of X_A. The spectrum of T_1 was fitted

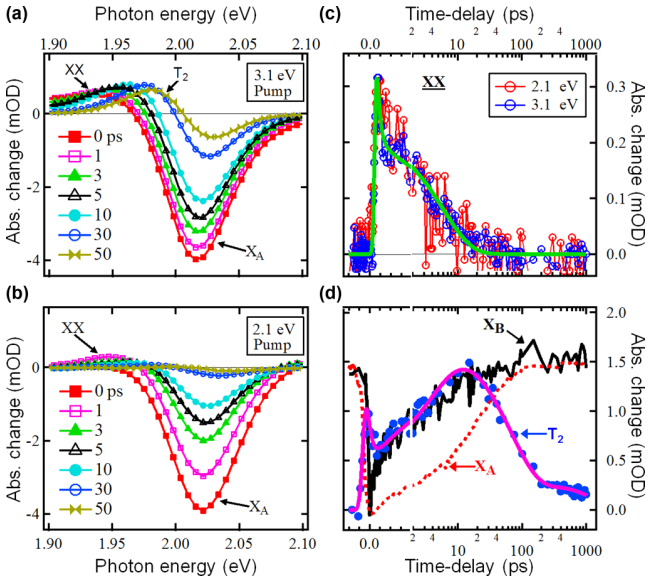

FIG. 2. (Color online) **Origins of T_2 and XX**. (**a**), TAS collected after excitation at 3.1 eV at time-delays as indicated. (**b**), TAS collected after excitation at 2.1 eV at time-delays as indicated. (**c**), Dynamics of XX plotted at 1.94 eV upon excitation at 3.1 and 2.1 eV, fit to a bi-exponential function (green solid line). The fitting parameters are listed in Table S3. For clarity, the signal amplitude in the case of excitation at 3.1 eV was divided by 2 which does not affect its dynamics. (**d**), Measured dynamics of T_2 upon excitation at 3.1 eV plotted at 1.98 eV (filled blue circle) fit to one exponential rise (3.7 ps time constant) and two exponential decays, see Table S3 (solid pink plot). The fitting parameters are listed in Table S3. For comparison, bleach recoveries of X_A and X_B upon excitation at 3.1 eV are plotted with their amplitudes normalized and shifted to match the amplitude of T_2 .

well to one Gaussian, but in the case of excitation at 3.1 eV, the fit of the induced absorption spectrum at 500 ps delay required two Gaussians [Fig. 1(d)]. During the fit of this spectrum, the width and center of T_1 were fixed, and the parameters of the second component (T_2) were returned by the fit [Fig. 1(d)]. These induced absorptions located at the "red" side of X_A may have several origins such as exciton-exciton and exciton–free - carrier collisional broadening of the excitonic absorption bands [26,27], biexciton formation [14,28], many-body interaction effects [28], intraband transitions [26], laser heating, neutral bound exciton trapping [29], or charge trapping [30]. However, some of these processes can be excluded based on the dynamics of these induced absorptions T_1 and T_2.

In order to identify the source of T_1- and T_2-induced absorptions, we examine the TAS collected at early time-delays (Fig. 2). Consistent with Fig. 1(d), T_2-induced absorption ~1.98 eV was observed only in the case of excitation at 3.1 eV [Fig. 2(a)]. Additionally, both sets of transient spectra contained a negative differential absorbance that indicates stimulated emission and depletion of X_A, as well as an early-time-delay photoinduced absorption (XX) feature at energies ~1.94 eV. Based on the dynamics of XX and T_2 shown in Figs. 2(c) and 2(d), respectively, these two features can be spectrally distinguished. In fact, XX was formed instantaneously and disappeared within ~20 ps after excitation, but T_2 was formed slowly and did not reach its maximum amplitude until 20 ps after excitation. Moreover, T_2 decays slowly, with portions of its amplitude surviving up to hundreds of picoseconds, but XX decays with a 6 ps time constant, which is even faster than that of X_A bleach recovery (~9 ps) (see Tables S1 and S3 in the Supplemental Material [18]). The XX absorption feature observed for both 2.1 eV and 3.1 eV pump excitations can be attributed to exciton-exciton and exciton–free-carrier collisional broadening of the excitonic absorption bands [26] and/or biexciton formation [14].

To eliminate the possibilities of changes in the oscillator strength due to shifts in exciton absorption, laser heating, and free-carrier generation, we carried out a control experiment. Transient absorption spectra were collected upon excitation of the same spot on the sample and under the same pump fluence (~2 μJ/cm^2) using two pump photon energies: 2.3 eV (insufficient for X_B generation) and 2.4 eV (sufficient for X_B generation). The resulting spectra shown in Figs. S7(a) and S7(b) in [18], demonstrate that T_2 was observed when the pump photon excitation energy was $\geqslant$2.4 eV, which matches the position of the X_B absorption band and the possible onset of the X_A continuum [23] and was not observed for the pump at 2.3 eV.

It is possible that the T_1- and T_2-induced absorption features indicate exciton absorption broadening shifts resulting from many-body interaction effects, such as exciton-exciton or exciton–free-carrier interactions [27,28,31]. In strongly confined systems, the absorption spectrum of photogenerated excitons can be broadened due to Coulomb interactions arising from many-body exciton-exciton repulsive interactions [27,28]. According to Fig. 1(c), excitons (X_A) disappeared within the first 100 ps following pump excitation; the clearly resolved spectral features measured at 500 ps in Fig. 2(d) should be devoid of such exciton-exciton or exciton–free-carrier interactions. Moreover, by 20 ps time-delay, more than 90% of exciton X_A bleach has recombined [see Fig. 1(d)], and at this same time delay the T_2 amplitude was the greatest [see Fig. 2(d)]. If T_2 originated from exciton-exciton and/or exciton–free-carrier interaction, one would expect the T_2 amplitude to be the greatest when X_A bleach amplitude is the highest. Similar arguments apply for intraband transitions; which should also be unlikely after 20 ps time-delay.

For the possibility of bound exciton trapping, one would expect the electron and hole to recombine at most within the same time scale as X_A because both electron and hole are trapped together and still bound to each other. Transient absorption results shown in Figs. 1(c) and 1(d) indicate that X_A lived less than 100 ps but T_1-and T_2-induced absorptions survived beyond 500 ps after excitation. Consequently, this possibility of bound exciton trapping can be ruled out.

In conclusion, based upon the above dynamics analysis and the control experiment of exciting at 2.3 and 2.4 eV, it is unlikely that the processes of laser heating, biexciton formation, many body interaction effects, neutral bound exciton trapping, or intraband transitions are viable explanations for the origin of the induced absorptions T_1 and T_2. A much more likely scenario for the long lifetimes observed for features T_1 and T_2 is photoinduced absorption arising from charge trapping of electrons or holes, a process that can last hundreds of

picoseconds, which is consistent with the spectra of T_1 and T_2 measured 500 ps after excitation as shown in Fig. 1(d).

In this scenario, we hypothesize that excitons X_A and X_B, generated by the pump pulse, dissociate through transferring their holes to trapping site (TS) that belong to the substrate or defects in the crystal, leaving their electrons in the CB to bind with electron-hole pairs generated by the probe pulse to form negative trion states (conversely, positive trion formation would involve electron trapping, and residual holes). Similar trion formation upon exciton dissociation has been observed in carbon nanotubes [30,32].

To test the hypothesis of trion generation through charge trapping, the dependence of T_1 and T_2 absorption on pump laser fluence was measured at 500 ps delay. According to Figs. S5 and S8 in the Supplemental Material [18], while X_A and X_B depletions saturate at $\sim 6\,\mu J/cm^2$ energy fluence, T_1- and T_2-induced absorption features saturate at $\sim 3\,\mu J/cm^2$ pump fluences, indicating that T_1 and T_2 amplitudes are more correlated with the number of available trapping sites rather than the production of X_A and X_B.

If T_1 and T_2 reflected the generation of positive trions due to electron trap states located within the band gap of 2D WS_2 monolayers, they would be populated as long as X_A or X_B is formed. According to the transient spectra shown in Fig. 1(d), T_2 was not observed in the case of excitation at 2.1 eV despite the fact that X_A was equally populated as in the case of excitation at 3.1 eV. Similarly, according to Fig. 1(d), the amplitude of T_1 resulting from excitation at 3.1 eV was only one-third of that occurring by excitation at 2.1 eV despite the fact that the amplitudes of the X_A bleach were the same [Fig. 1(c)]. Consequently, it is unlikely that T_1 and T_2 are positive trions that originate by optically p-doping WS_2 as a consequence of trapping electrons by the substrate or defect sites. However, in the alternative case where X_A and X_B undergo dissociation via holes trapping to substrate or defect sites, essentially optically doping the semiconductor n type, excitation by the probe pulse may lead to the formation of negative trions.

To check this hypothesis we carried out electro-optical spectroscopy (EOS) measurements (Fig. 3). When introducing excess electrons into the CB upon the application of positive voltages, static absorbance change spectra (comparing bias on/off) exhibited an induced absorption similar to T_2. Furthermore, as the n-doping level increased with increasing bias, the amplitude of this feature increased. A corresponding induced absorbance similar to T_1 was not observed, probably due to the close spectral overlap between the positions of absorption of T_1 and the bleach of X_A. Note that in the femtosecond transient measurements, T_1 became observable only after the X_A bleach had completely disappeared [Fig. 1(d)], but in static EOS measurements, possible T_1 absorbance is unresolvable due to the strong X_A bleach. It should be noted additionally, that in the EOS measurements the substrate was SiO_2/Si while in the femtosecond pump-probe experiments, the substrate was sapphire. Upon application of negative voltages, which consists of introducing excess holes into the VB, the resulting absorbance spectrum was completely different than previously measured for T_1 and T_2. It contained a spectrally broad induced absorption that is different from T_1 and T_2 observed in Fig. 1(d), which may indicate the generation of positive trion states.

Because in these experiments trions form as a result of photoabsorption involving a free electron resulting from exciton formation and dissociation, in the case of excitation at 2.1 eV, T_1 should originate from photodoping resulting from dissociation of X_A. However, in the case of pumping at 3.1 eV, both X_A and X_B excitons as well as free electrons and holes are generated, which allowed the photoformation of both T_1 and T_2 by the probe light. Note that the amplitude of T_1 was one-third that using the pump at 2.1 eV.

Within the framework of T_1 and T_2 photogeneration via holes transfer to a trapping site belonging to the substrate of defects in the crystal, the ambiguous dependence of the X_A bleach recovery dynamics on the excitation energy, observed in Fig. 1(c), can be explained according to a mechanism of trion photogeneration as depicted in Fig. 4. Upon pump laser excitation at 2.1 eV, where only X_A is generated, the faster X_A bleach recovery is attributed to more efficient transfer of

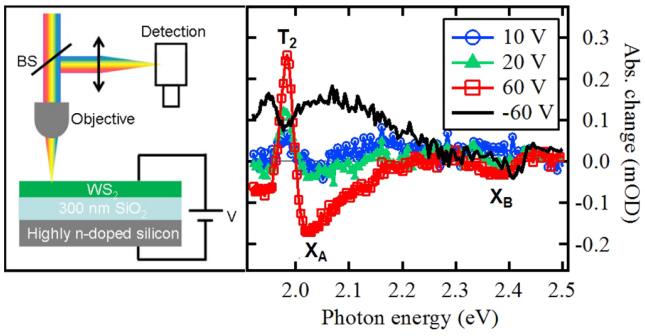

FIG. 3. (Color online) Scheme representative for the experimental setup used for electro-optical static transient absorption measurements (left panel), and absorbance change spectra at different n-doping levels as indicated (right panel).

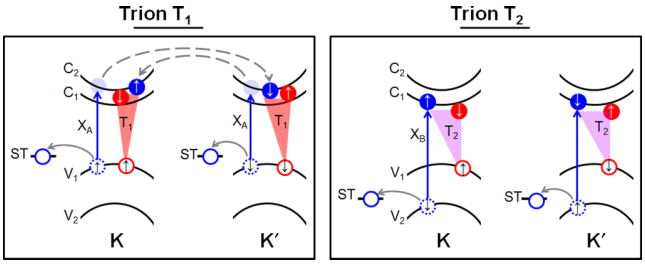

FIG. 4. (Color online) **Mechanism of T_1 and T_2 generation at the K and K′ points in a pump-probe experiment**. (Left panel) Exciton X_A (blue circles) is generated upon quasi-resonant excitation with respect to X_A by the pump pulse. Following dissociation of X_A (at both K and K′) through hole trapping at the substrate or a defect site (ST), the remaining electron at the K(K′) valley joins (dashed arrows) the newly generated electron-hole pairs (red circles) by the probe at K′(K) to form T_1. (Right panel) Upon generation of exciton X_B (blue circles) using sufficient pump photon energy, and following its dissociation through hole trapping at ST, the remaining electron at C_1 binds to the newly generated electron-hole pairs (red circles) through the $V_1 \rightarrow C_1$ trion transition upon absorption of probe photons. To account for T_1 and T_2 binding energies, they are depicted lower than C_2 and C_1 levels, respectively.

the X_A -hole to the trapping site, which also produced more T_1. Indeed according to Fig. 1(d), the amount of generated T_1 following pumping at 2.1 eV was three times that for excitation at 3.1 eV.

Depicted in Fig. 4 is a cartoon representation for the mechanism of T_1 and T_2 generation in these pump-probe experiments. Upon near-resonant excitation with respect to X_A, the generated excitons dissociate via hole trapping at trapping sites on adsorbates or on the substrate, and T_1 is generated as follows: the remaining electron with spin state down (up) $|e\downarrow\rangle$ ($|e\uparrow\rangle$) at the $K(K')$ valley binds to the newly generated electron-hole pair $|h\downarrow e\uparrow\rangle$ ($|h\uparrow e\downarrow\rangle$ at the $K'(K)$ valley upon absorption of probe photons to form T_1. Noting that this photogenerated trion T_1 is in its ground state $|h\uparrow e\downarrow e\uparrow\rangle$ [33] at the K valley and $|h\downarrow e\uparrow e\downarrow\rangle$ at the K' valley. In the case of excitation with photon energies $\geqslant$2.4 eV (sufficient for X_B generation and possible production of free carriers), the X_B dissociation through hole trapping leaves a free electron $|e\uparrow\rangle$ ($|e\downarrow\rangle$) at the $K(K')$ valley, which binds to the electron-hole pair $|h\uparrow e\downarrow\rangle$ ($|h\downarrow e\uparrow\rangle$) generated by the probe pulse to form T_2 in its ground state at the $K(K')$ valleys through the trionic transition. We note that, in the absence of the photodoping electron at C_1, an excitonic transition $V_1\rightarrow C_1$ is optically forbidden. In this case, population of both C_1 and C_2 in the CB is possible, but the exclusivity of T_1 and T_2 photogeneration is controlled by Pauli blocking at V_1 in the VB.

Although it is possible to generate T_2 even upon pumping below X_B due to intervalley spin flip [21] of X_A's remaining electron, which crosses the valley to C_1, and can bind to electron-hole pairs generated by the probe through the trionic transition across $V_1\rightarrow C_1$ to form T_2, we did not observe it, possibly due to Pauli blocking at V_1, because this level is already occupied by the T_1 hole. Also, in transient absorption spectra, one would expect to see an additional induced absorption near X_B reflecting the generation of a trion through the trionic transition across $V_2\rightarrow C_1$. Our measurements did not indicate the formation of this trion, which is consistent with EOS experiments where even at high n doping (see Fig. 3), no noticeable induced absorption to the red side of X_B was observed. This is in accordance with recent reports of low-temperature static photoluminescence under external n doping [6].

IV. CONCLUSION

In summary, ultrafast pump-probe spectroscopy of 2D WS_2 monolayers identified two spectral absorption peaks that we attribute to different negative trions. The mechanisms and dynamics for their photogeneration were revealed by monitoring the characteristic absorption bands and dynamics of the two lowest excitons, X_A and X_B, for different pump laser wavelengths. Pump laser photon energies <2.4 eV, sufficient to create only the X_A exciton, result in a single photoinduced absorption band centered at ~2.02eV (25 meV FWHM) that we attribute to trion states T_1, which are bound by ~10 meV with respect to X_A, in good agreement with Ref [14]. This photoabsorption to create trions persists for ~1 ns and correlates with the bleach recovery time of X_A, from which we conclude that free electrons that are necessary to enable trion formation likely arise from exciton dissociation, enabled by hole trapping at defect sites in the WS_2 crystal or the substrate which persist for these characteristic times.

A second photoinduced absorption peak at 1.98 eV, with ~18 meV FWHM appears when $\lambda_{pump} > 2.4$ eV, energies that are just sufficient to excite the X_B exciton, which we conclude is correlated with a second negative trion state T_2. The correlation between T_2 formation dynamics and X_B bleach recovery dynamics suggests that it can be similarly generated by the dissociation of exciton X_B (and higher excitons or free electron-hole pairs) into free electrons and trapped holes. In support of the hypothesis that the photoinduced absorbing species are negative trions forming as a consequence of n-type photodoping, a similar photoinduced absorption feature to T_2 was observed by externally n-doping the sample, the amount of generated T_2 increasing with increasing doping level. However, the spectral position of the T_2 band is 420 meV below the X_B transition (V_2-C_1), suggesting that it corresponds to a trion state with a binding energy of 17 ± 2.8 meV with respect to a "dark exciton" corresponding to a transition (V_1-C_1) that is forbidden by spin selection rules.

Because the holes of T_1 and T_2 occupy the same valence band level (V_1), the formation of the two trions should undergo a Pauli blocking competition process, which is consistent with our observation that T_1 decreases by two-thirds when T_2 is formed.

These findings highlight the strong role that charge trapping sites from substrates or adsorbates can play in affecting the excitonic transitions in 2D TMD monolayers, and in the formation of quasiparticles such as trions. For instance, it should be possible to control the formation and lifetime of trapped charges, and thus the time window for trion photogeneration, through selectively designing appropriate substrate architectures. The ability to adjust the photogeneration of additional optically active band-edge excitonic states opens an additional perspective for many-body physics at the fundamental science level, and it may boost optoelectronic applications based on 2D TMDs, notably photovoltaics and information technology.

ACKNOWLEDGMENTS

This research was conducted at the Center for Nanophase Materials Sciences, which is a DOE Office of Science User Facility. This research used resources of the National Energy Research Scientific Computing Center, a DOE Office of Science User Facility supported by the Office of Science of the U.S. Department of Energy under Contract No. DE-AC02-05CH11231.

A.B. and B.H. contributed equally to this work. All the authors discussed and approved this work.

[1] H. A. Bethe and E. E. Salpeter, *Quantum Mechanics of One and Two Electron Atoms* (Springer, Berlin, 1957), p. 154.

[2] A. J. Shields, J. L. Osborne, M. Y. Simmons, M. Pepper, and D. A. Ritchie, Phys. Rev. B **52**, R5523 (1995).

[3] H. Buhmann, L. Mansouri, J. Wang, P. H. Beton, N. Mori, L. Eaves, M. Henini, and M. Potemski, Phys. Rev. B **51**, 7969(R) (1995).

[4] M. A. Lampert, Phys. Rev. Lett. **1**, 450 (1958).

[5] A. Chernikov, T. C. Berkelbach, H. M. Hill, A. Rigosi, Y. Li, Ö. B. Aslan, D. R. Reichman, M. S. Hybertsen, and T. F. Heinz, Phys. Rev. Lett. **113**, 076802 (2014).

[6] Z. Ye, T. Cao, K. O'Brien, H. Zhu, X. Yin, Y. Wang, S. G. Louie, and X. Zhang, Nature (London) **513**, 214 (2014).

[7] K. F. Mak, K. He, C. Lee, G. H. Lee, J. Hone, T. F. Heinz, and S. Jie, Nat. Mater. **12**, 207 (2013).

[8] A. M. Jones, H. Yu, N. J. Ghimire, S. Wu, G. Aivazian, J. S. Ross, B. Zhao, J. Yan, D. G. Mandrus, D. Xiao, W. Yao, and X. Xu, Nat. Nanotechnol. **8**, 634 (2013).

[9] S. Narita and M. Taniguchi, Phys. Rev. Lett. **36**, 913 (1976).

[10] K. S. Novoselov, A. K. Geim, S. V. Morozov, D. Jiang, Y. Zhang, S. V. Dubonos, I. V. Grigorieva, and A. A. Firsov, Science **306**, 666 (2004).

[11] D. Xiao, M. C. Chang, and Q. Niu, Rev. Mod. Phys. **82**, 1959 (2010).

[12] N. Nagaosa, J. Sinova, S. Onoda, A. H. MacDonald, and N. P. Ong, Rev. Mod. Phys. **82**, 1539 (2010).

[13] W. Yao, D. Xiao, and Q. Niu, Phys. Rev. B **77**, 235406 (2008).

[14] J. Shang, X. Shen, C. Cong, N. Peimyoo, B. Cao, M. Eginligil, and T. Yu, ACS Nano **9**, 647 (2015).

[15] Y. Zhang, Y. Zhang, Q. Ji, J. Ju, H. Yuan, J. Shi, T. Gao, D. Ma, M. Liu, Y. Chen, X. Song, H. Y. Hwang, Y. Cui, and Z. Liu, ACS Nano **7**, 8963 (2013).

[16] G. Kresse and J. Furthmuller, Comput. Mater. Sci. **6**, 15 (1996).

[17] M. Shishkin and G. Kresse, Phys. Rev. B **74**, 035101 (2006).

[18] See Supplemental Material at http://link.aps.org/supplemental/10.1103/PhysRevB.92.115443 for additional experimental results, analysis and discussions.

[19] J. A. Wilson and A. D. Yoffe, Adv. Phys. **18**, 193 (1969).

[20] B. Zhu, X. Chen, and X. Cui, Sci. Rep. **5**, 9218 (2015).

[21] C. Mai, Y. G. Semenov, A. Barrette, Y. Yu, Z. Jin, L. Cao, K. W. Kim, and K. Gundogdu, Phys. Rev. B **90**, 041414(R) (2014).

[22] J. Kang, S. Tongay, J. Zhou, J. Li, and J. Wu, Appl. Phys. Lett. **102**, 012111 (2013).

[23] T. Stroucken and S.W. Koch, J. Phys.: Condens. Matter **27**, 345003 (2015).

[24] D.Y. Qiu, F. H. da Jornada, and S. G. Louie, Phys. Rev. Lett. **111**, 216805 (2013).

[25] H. R. Gutierrez, N. Perea-Lopez, A. L. Elías, A. Berkdemir, B. Wang, R. Lv, F. Lopez-Urías, V. H. Crespi, H. Terrones, and M. Terrones, Nano Lett. **13**, 3447 (2013).

[26] H. Shi, Y. Yan, S. Bertolazzi, J. Brivio, B. Gao, A. Kis, D. Jena, H. G. Xing, and L. Huang, ACS Nano **7**, 1072 (2013).

[27] S. Sim, J. Park, J. G. Song, C. In, Y. S. Lee, H. Kim, and H. Choi, Phys. Rev. B **88**, 075434 (2013).

[28] C. Mai, A. Barrette, Y. Yu, Y. G. Semenov, K. W. Kim, L. Cao, and K. Gundogdu, Nano Lett. **14**, 202 (2014).

[29] T. Kato and T. Kaneko, ACS Nano **8**, 12777 (2014).

[30] S. M. Santos, B. Yuma, S. Berciaud, J. Shaver, M. Gallart, P. Gilliot, L. Cognet, and B. Lounis, Phys. Rev. Lett. **107**, 187401 (2011).

[31] D. Sun, Y. Rao, G. Reider, G. Chen, Y. You, L. Brezin, A. R. Harutyunyan, and T. F. Heinz, Nano Lett. **14**, 5625 (2014).

[32] A. M. Dowgiallo, K. S. Mistry, J. C. Johnson, and J. L. Blackburn, ACS Nano **8**, 8573 (2014).

[33] P. Michler, *Single Semiconductor Quantum Dots* (Springer, Berlin, 2009), pp. 78–81.